Chemical Science

ROYAL SOCIETY OF CHEMISTRY

EDGE ARTICLE

View Article Online
View Journal | View Issue

Cite this: *Chem. Sci.*, 2020, **11**, 7070

All publication charges for this article have been paid for by the Royal Society of Chemistry

Received 25th March 2020
Accepted 16th June 2020

DOI: 10.1039/d0sc01749c

rsc.li/chemical-science

Efficient and selective alkene hydrosilation promoted by weak, double Si–H activation at an iron center†

Patrick W. Smith, ‡ Yuyang Dong § and T. Don Tilley *

Cationic iron complexes $[Cp^*(^iPr_2MeP)FeH_2SiHR]^+$, generated and characterized in solution, are very efficient catalysts for the hydrosilation of terminal alkenes and internal alkynes by primary silanes at low catalyst loading (0.1 mol%) and ambient temperature. These reactions yield only the corresponding secondary silane product, even with SiH_4 as the substrate. Mechanistic experiments and DFT calculations indicate that the high rate of hydrosilation is associated with an inherently low barrier for dissociative silane exchange (product release).

Introduction

Olefin hydrosilation is one of the most commercially important reactions, used to produce various silicon-containing materials and fine chemicals.[1,2] As practiced, this reaction mainly employs Pt-based catalysts[3,4] which, given the limited supply and high demand for platinum, creates a strong motivation for development of alternative catalysts based on more earth-abundant metals such as Fe, Co, and Ni.[5–22] There are profound differences between the chemical properties of Pt and those of the base metals; most notably the lighter 3d metals have a higher propensity for one-electron reaction steps, which may preclude the oxidative addition/reductive elimination cycles associated with noble metal catalysis. For this reason, the search for base metal hydrosilation catalysts must include discovery of alternative mechanistic pathways suitable for the 3d metals.[23]

Previous work in this laboratory identified a new mechanism for hydrosilation[24,25] associated with cationic silylene complexes of Ru[24,26] and Ir.[27] Unique to this mechanism is the Si–C bond forming step, in which a Si–H bond in a silylene ligand directly adds across the olefin.[2,28] This process is attractive for the design of new hydrosilation catalysts based on 3d metals such as iron, as this critical bond formation does not rely on a metal-centered redox process. Hydrosilation reactions catalyzed by cationic silylene complexes form secondary silane products with linear regioselectivity for the Si–H addition. This selectivity represents an advantage over the more conventional Chalk–Harrod mechanism, which can result in a mixture of linear and branched products due to its reliance on reversible olefin insertion into a metal hydride.

Another aspect of a silylene-based mechanism is the double Si–H bond activation that occurs at the metal center.[25,30] Double Si–H activations of this type occur to varying degrees, from moderate activation to give η^3-silane complexes (**A**, Scheme 1),[30–32] to more strongly activated cases that have undergone a double oxidative addition to form a silylene dihydride (**B**, **C**).[26,33–35] Structures along this continuum exhibit high electrophilicity at silicon and greater reactivity for the terminal Si–H bond.

Since the silylene-based mechanism is well established for ruthenium complexes of the type $[Cp^*(^iPr_3P)Ru(H)_2SiHR]^+$, catalytic transformations with analogous iron complexes could provide increased activity due to the enhanced lability of metal–

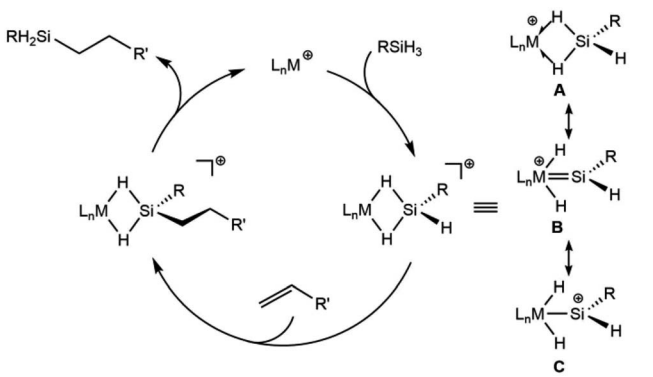

Scheme 1 Representation of the cationic silylene mechanism for hydrosilation with three selected resonance structures for the cationic complexes.

Department of Chemistry, University of California, Berkeley, Berkeley, California 94720-1460, USA. E-mail: tdtilley@berkeley.edu

† Electronic supplementary information (ESI) available: Experimental details, characterization data, and computational details (PDF). See DOI: 10.1039/d0sc01749c

‡ Current address: Department of Chemistry, Massachusetts Institute of Technology, Cambridge, Massachusetts 02139, USA.

§ Current address: Department of Chemistry and Chemical Biology, Harvard University, 12 Oxford Street, Cambridge, Massachusetts 02138, USA.

ligand bonds in 3d complexes. This report describes the utility of Cp*(^{i}Pr$_2$MeP)FeH(N$_2$)[36] (**1**) as a precatalyst for alkene hydrosilation *via* generation of a cationic iron intermediate. This Fe system is associated with higher rates of conversion for many substrates, and a marked selectivity toward terminal olefins that underscores fundamental mechanistic differences with the related Ru catalyst.

Results and discussion

Precursors to the catalytic species of interest are neutral iron complexes of the type Cp*(^{i}Pr$_2$MeP)Fe(H)$_2$SiH$_2$R. Compound **1** reacts with primary silanes (RSiH$_3$, R = Trip,[37] Ph, *p*-Tol, Mes; Trip = 2,4,6-triisopropylphenyl) by oxidative addition of an Si–H bond to form the corresponding dihydrides Cp*(^{i}Pr$_2$MeP)Fe(H)$_2$SiH$_2$R (**2$_R$**, eqn (1)). Note that related half-sandwich complexes have been reported previously.[36,38,39] These silyl dihydride complexes do not promote hydrosilations up to 80 °C, but they are converted to active cationic catalysts by hydride abstraction.

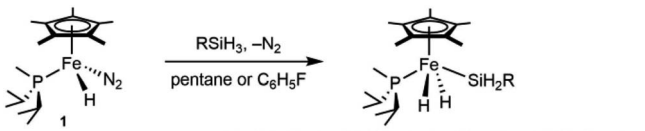

R = Ph (**2$_{Ph}$**), *p*-Tol (**2$_{Tol}$**), Cy, Mes (**2$_{Mes}$**), Trip (**2$_{Trip}$**) (1)

The cationic complex [Cp*(^{i}Pr$_2$MeP)FeH$_2$SiHPh][BAr$^F_4$] (**3$_{Ph}$**; BAr$^F_4$ = tetrakis(pentafluorophenyl)borate) was generated by treatment of **1** with 1000 equiv. of PhSiH$_3$ followed by 1 equiv. [Ph$_3$C][BAr$^F_4$] in fluorobenzene at −35 °C. After warming to ambient temperature, treatment with 1100 equiv. of 1-octene resulted in quantitative conversion of the silane substrate over 6 h to the linear product Ph(^{n}Oct)SiH$_2$ (eqn (2)), corresponding to a turnover frequency (TOF) of at least 170 h^{-1}. This selectivity toward primary silanes is reminiscent of the cationic Ru silylene hydrosilation catalyst, but other selectivities (*vide infra*) suggest that there are fundamental differences in the mechanistic pathways.[24,26,28,29] For this reaction the iron catalyst is more active, as the ruthenium catalyst required a higher loading (1 mol%) and elevated temperature (80 °C) to achieve a comparable conversion.[26] This activity is in the range of the most active iron catalysts for the hydrosilation of olefins by primary silanes (Table S1†).[22,40–43]

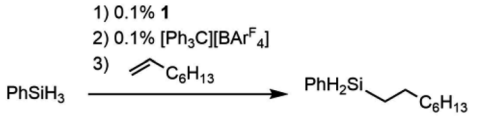

(2)

Aryl- and alkyl-substituted primary silanes are suitable substrates for this catalysis (Table 1), but steric factors play an important role. While (*o*-ethylphenyl)silane is a competent substrate, hydrosilation of 4-methylpentene with mesitylsilane did not proceed even at 80 °C. No hydrosilation products were observed with secondary or tertiary silanes (*e.g.* PhMeSiH$_2$ and Et$_3$SiH) up to 1 mol% catalyst loading over 20 h at ambient temperature. Unlike the Ru silylenes, the Fe catalysts are highly

Table 1 Silane scope for hydrosilation of 4-methylpentene. Conditions: fluorobenzene, 0.1 mol% **1**, 0.1 mol% [Ph$_3$C][BAr$^F_4$], ambient temperature

	Silane	Product	Time (h)	Yield[a]
a	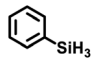	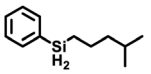	6	>98
b	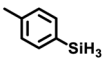	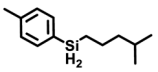	20	>98
c		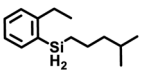	20	>98
d	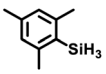	N. R.	20	0[b]
e	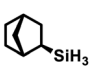	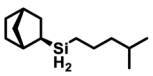	20	>98

[a] Isolated yield. [b] Silane redistribution observed at 80 °C.

Table 2 Olefin and alkyne scope for hydrosilation by PhSiH$_3$. Conditions: fluorobenzene, 0.1 mol% **1**, 0.1 mol% [Ph$_3$C][BAr$^F_4$], ambient temperature

	Alkene/alkyne	Product	Time (h)	Yield[a]
f	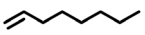	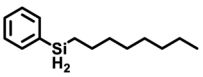	6	>98
g		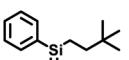	0.5	95 (97)
h		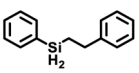	20	97 (98)
i	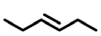	N. R.	20	0
j		N. R.	20	0
k	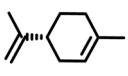	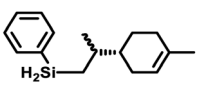	20	92 (97)[b]
l		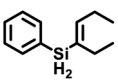	5	87 (95)
m	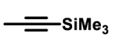		20	89 (97)[c]
n	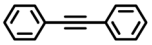	N. R.	20	0
o		N. R.	20	0

[a] Isolated yield (NMR yield). [b] Diastereomeric excess = 15%. [c] R = Me, R′ = SiMe$_3$, 87.5%; R = SiMe$_3$, R′ = Me, 12.5%.

selective toward hydrosilation of terminal olefins (Table 2). This difference in substrate tolerance may arise from the size difference between ruthenium and iron, resulting in greater steric demands from the Fe ancillary ligands in the hydrosilation transition state, and is most dramatically illustrated by the hydrosilation of limonene (entry *k*) which resulted in complete selectivity for the terminal double bond.

The iron catalysts selectively give *cis*-hydrosilation of internal alkyne substrates (entries l and m; Table 2, by ^{1}H NMR spectroscopy), which is consistent with direct Si–H addition. No conversion was observed for diphenylacetylene (entry n), presumably due to steric factors, and further evidence that catalyst selectivity is driven by steric factors is seen with propynyltrimethylsilane as substrate, to predominantly form 2-phenylsilyl-1-trimethylsilylpropene (~90% selectivity). The intolerance for the terminal acetylenic substrate (entry o) is most likely due to side reactions with the acetylenic C–H bond.

The selectivity of this catalyst system suggested the use of SiH_4 to form secondary silanes (eqn (3)). For this reaction, the catalyst was generated by reaction of $\mathbf{2_{Mes}}$ with $[Ph_3C][BAr^F{}_4]$ in fluorobenzene, which was then treated with 400 equiv. of 4-methylpentene and exposed to 1 atm of 15% silane in nitrogen. While the yield of (4-Me-pentyl)$_2SiH_2$ was only 2.6% after 18 h (based on olefin; TON = 52), the reaction is highly selective in that only the secondary silane was observed as product (by ^{1}H NMR spectroscopy and TLC). The low yield is attributed to the low concentration of SiH_4; higher pressures of silane and longer reaction times would likely give greater turnover.

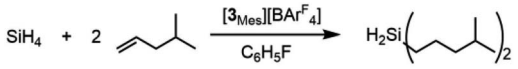

(3)

Attempts to isolate the activated catalysts as crystalline solids were not successful; in all cases, crystallization attempts produced impure oils, prompting characterization *in situ* by NMR spectroscopy. Complex $\mathbf{2_{Tol}}$ was treated with 1 equiv. of $[Ph_3C][BAr^F{}_4]$ at −35 °C in fluorobenzene in an attempt to generate $[Cp^*(^iPr_2MeP)FeH_2SiH(p\text{-Tol})]^+$ ($\mathbf{3_{Tol}}$, eqn (4)), which resulted in a color change to blue. Integration against a C_6Me_6 internal standard indicated that $\mathbf{3_{Tol}}$ was formed in >99% yield. The ^{1}H NMR spectrum at room temperature did not contain obvious Fe–H–Si or Si–H resonances, suggesting the possibility of exchange between such positions. Upon cooling a solution of $\mathbf{3_{Tol}}$ in fluorobenzene-d_5 to −30 °C, Fe–H (−15.12 ppm, J_{HP} = 20.9 Hz, $J_{Si(\mu\text{-}H)}$ = 90 Hz) and Si–H (6.74 ppm, J_{SiH} = 180 Hz) resonances were observed. These resonances display cross peaks to a downfield ^{29}Si resonance at 188 ppm in the HMBC spectrum ($J_{Si(\mu\text{-}H)}$ 90 Hz).

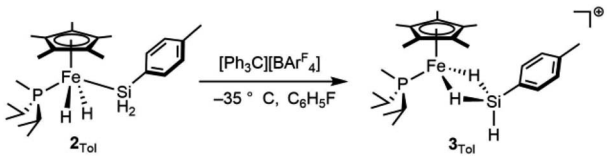

(4)

Computations on the structure of $\mathbf{3_{Ph}}$ were found to be highly dependent upon the choice of functional, particularly with respect to the extent of Si–H activation at the Fe center. The experimentally determined structure of the related Ru complex, $[Cp^*(^iPr_3P)Ru(H)_2{=}Si(H)Mes]^+$, was used to calibrate the choice of functional, and the range-separated-hybrid functional ωB97X-D3 was found to be in best agreement with this structure. For the Fe complex, calculations at the ωB97X-D3/def2-TZVP/SVP level of theory are consistent with the interpretation that Si–H activation at Fe is modest. The geometry of the molecule resembles an η^3-silane structure (Fig. 1), with the hydrides symmetrically bridging the Fe and Si atoms and minimal Si–H activation relative to free silane (d_{FeSi} = 2.20 Å; FSR = 0.95). The Si–H$_{(bridge)}$ distances are slightly longer than the terminal Si–H distance (1.59 *vs.* 1.47 Å) and the Fe–H distances average to 1.68 Å (FSR = 1.14). The FeH_2Si unit is planar ($\Sigma_\angle$ = 358°). In contrast, $[Cp^*(^iPr_2MeP)RuH_2SiHPh]^+$ ($\mathbf{3_{RuPh}}$) is computed to have proceeded significantly further along the double Si–H activation continuum, and toward a structure that may be regarded as a silylene dihydride. To wit, $\mathbf{3_{RuPh}}$ is computed to possess an extremely short Ru–Si distance (2.25 Å; FSR = 0.93), Si–H$_{(bridge)}$ distances which are elongated relative to those in $\mathbf{3_{Ph}}$ (1.67 Å), and short Ru–H interactions (1.75 Å; FSR = 1.11).

The selectivity of the Fe catalysts with respect to the olefin substrates prompted an investigation into the hydrosilation mechanism. For $[Cp^*(^iPr_3P)RuH_2SiHR]^+$, the rate-limiting step in catalysis is the dissociative exchange of the product silane with silane substrate.[26] For the corresponding osmium complexes, catalytic activity was not observed, even though

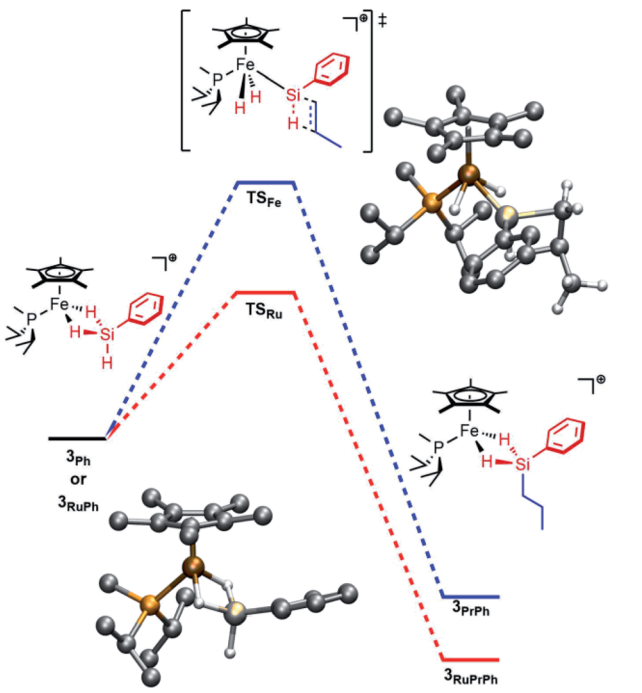

Fig. 1 Computed energy profile for addition of propylene to $\mathbf{3_{Ph}}$ (blue) or $\mathbf{3_{RuPh}}$ (red). Bottom left: computed structure of $\mathbf{3_{Ph}}$. Top right: computed structure of $\mathbf{TS_{Fe}}$.

stoichiometric Si–H addition to olefins proceeds rapidly.[24,44] This suggests that dissociative silane exchange is even less favorable for Os. In light of this trend toward lower barriers to silane exchange from Os to Ru, a reasonable hypothesis is that the barrier to silane exchange for Fe is even lower, to the extent that the rate of direct Si–H addition to the olefin may become competitive. This would explain both the increased activity of the Fe catalysts for unhindered substrates and the sterically-based selectivity for terminal olefins.

This hypothesis is supported by computational investigations of the catalytic cycle using geometries calculated at the ωB97X-D3/def2-TZVP/SVP level of theory, with single point energies corrected at the DLPNO-CCSD(T)/def2-TZVP level of theory. The computed energy profile for the olefin addition (Fig. 1) indicates that the transition state for Si–H addition to the olefin (**TS**) is at a higher energy than that for the Ru system ($\Delta G^{\ddagger}$ = 19.1 kcal mol^{-1} for Fe *vs.* 11.7 kcal mol^{-1} for Ru; previous computations indicated a 8–15 kcal mol^{-1} barrier for Ru).[28,29] Importantly, this barrier height is comparable to that of silane exchange (*vide infra*), and a consequence is that the rate-determining step for catalysis is substrate dependent. Thus, in at least some cases the Si–H addition is slow enough (*e.g.*, due to steric factors) to render this step rate-determining. This substrate-dependent reactivity could explain the novel selectivity of this Fe system.

Notably, while the $\mathbf{3_{Ph}}$ ground state involves bridging Fe–H–Si interactions, the Si–H interactions are considerably weaker in transition state $\mathbf{TS_{Fe}}$, manifested in elongation of the Si–H_{Fe} interactions from 1.59 to 1.89 Å, and shortening of the Fe–H (from 1.68 to 1.52 Å; ΔFSR = −0.11) and Fe–Si (from 2.20 to 2.15 Å; ΔFSR = −0.02) distances, consistent with generation of an electrophilic silylene in this transition state by a "double α-migration".[45]

A dissociative mechanism for silane exchange is supported by VT NMR spectroscopy. The complex [Cp*(^{i}Pr$_2$MeP)FeH_2-SiH(*p*-Tol)][BAr^{F}_4] ($\mathbf{3_{Tol}}$) was generated in fluorobenzene solution in the presence of 1 equiv. of *p*-tolylsilane, and the tolyl CH_3 and silane SiH_3 ^{1}H NMR resonances were monitored from 246 to 330 K. Above 290 K, the resonances attributed to free and bound *p*-TolSiH_3 broaden and coalesce, consistent with chemical exchange between the two species. Rate constants for the exchange between *p*-tolylsilane and $\mathbf{3_{Tol}}$ were determined based on lineshape analyses of the *p*-CH_3 resonances; an Eyring plot gave the activation parameters $\Delta H^{\ddagger}$ = 27.0(4) kcal mol^{-1} and $\Delta S^{\ddagger}$ = 34(1) cal mol^{-1} K^{-1} ($\Delta G^{\ddagger}_{295}$ = 17(2) kcal mol^{-1} at 298 K; see ESI†). These activation parameters are consistent with a dissociative exchange mechanism similar to that proposed for the Ru silylene system ($\Delta H^{\ddagger}$ = 32(2) kcal mol^{-1} and $\Delta S^{\ddagger}$ = 19(1) cal mol^{-1} K^{-1}, $\Delta G^{\ddagger}_{295}$ = 26(2) kcal mol^{-1}). The somewhat lower enthalpy of activation for Fe likely reflects the weaker bonding of the η^3-H_3SiR ligand to the metal, and the lower activation of the Si–H bonds in the Fe system relative to Ru.

Computationally, the dissociative mechanism for silane exchange involving the coordinatively unsaturated intermediate Cp*(^{i}Pr$_2$MeP)Fe^{+} (**I**, Fig. 2) is reasonable. This structure includes an agostic interaction with one of the phosphine ^{i}Pr substituents, as evidenced by a close contact with a C-bound H atom (d_{FeH} = 1.943 Å). Additionally, the triplet state for **I** is lower in energy than the singlet state by 12.5 kcal mol^{-1} suggesting a two-state mechanism for dissociative silane exchange at Fe in this system. In the triplet structure, the Fe–H distance in the agostic interaction is shorter (d_{FeH} = 1.893 Å). Notably, this situation is not observed computationally for [Cp*(^{i}Pr$_2$MeP)Ru]$^{+}$, for which the triplet state is higher in energy than the singlet state by 18.1 kcal mol^{-1}. A minimum energy crossing point (MECP) was found along the reaction coordinate for silane dissociation from $\mathbf{3_{Ph}}$. Note that the MECP computed using the ωB97X-D3 functional most likely does not reproduce either the energy or geometry of the MECP well, as this functional overstabilizes triplet states in both the present and related systems.[37] Thus, using the B3LYP functional (for which the singlet-triplet gap of **I** agrees much better with DLPNO-CCSD(T)) the MECP is found to be 4.6 kcal mol^{-1} above $\mathbf{3_{Ph}}$, and still lower in energy than the fully dissociated triplet species. In this structure, the Fe–Si bond has lengthened by *ca.* 0.2 Å, and one of the ^{i}Pr-Me groups from the phosphine has approached the Fe center.

While we were unable to fully optimize a transition state structure for silane dissociation, nudged elastic band (NEB) calculations of the silane dissociation coordinate indicate a very late transition state for the triplet state of **I** (Table S4†). Thus, the energetics of this intermediate can be used as a proxy for activation energies for silane dissociation; these energies are summarized in Table S3.† For dissociation to the triplet state of **I**, ΔH = 22.7 kcal mol^{-1} and ΔS is extremely positive (52.7

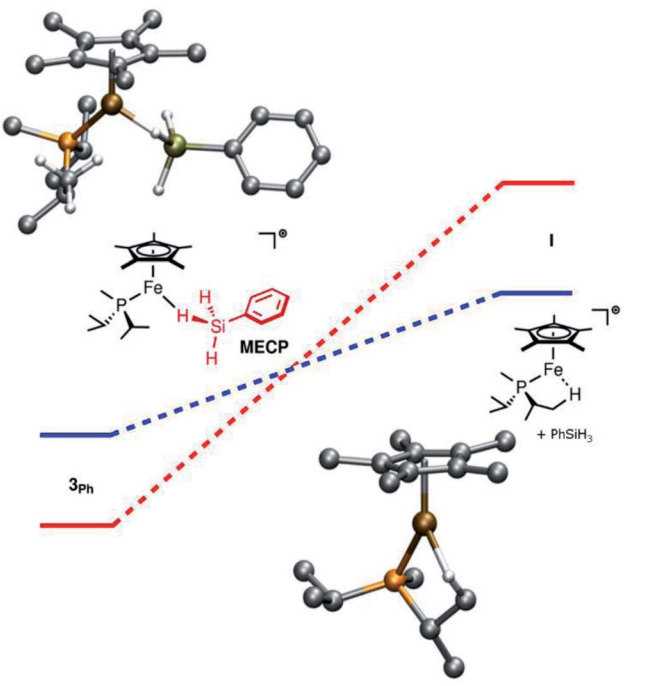

Fig. 2 Computed energy profile for the dissociation of silane from $\mathbf{3_{Ph}}$. The singlet pathway is shown in red, and the triplet pathway is shown in blue. Top left: structure of the MECP (minimum-energy crossing point). Bottom right: structure of the triplet state of **I**. Both structures were computed at the ωB97X-D3/def2-TZVP/SVP level of theory.

cal mol K^{-1}). However, since the true transition state for dissociation likely involves a closely-associated silane···**I** pair, all the translational and rotational entropy from dissociation will not have manifested in the Eyring analysis. Additionally, MECPs prior to the transition state can result in inefficient spin crossover, which should lead to a decrease in the rate relative to that of an analogous one-state process. These factors would result in a less positive experimental $\Delta S^{\ddagger}$ in an Eyring analysis.

Conclusions

The cationic Fe catalysts described here are highly active in the hydrosilation of unhindered olefins with primary silanes. This discovery provides the foundation for new catalyst design strategies involving the first-row transition metals. Importantly, the mechanistic pathway for these catalysts is non-oxidative in character, in that distinct oxidative additions are not required. The observed rate accelerations and enhanced selectivities relative to a related Ru system highlight the distinctly different catalysis that is possible for the 3d metals. In this case, mechanistic studies suggest that the promising characteristics of the iron catalysts relate to a *modest* degree of Si–H bond activation in the silane substrate, and therefore weaker metal–silane binding and a faster dissociative exchange of the product silane for the silane substrate. The lower cost and greater sustainability of Fe makes the present system highly attractive for the synthesis of unsymmetrical secondary silanes, and multiply-substituted silicon centers derived therefrom.

Conflicts of interest

There are no conflicts to declare.

Acknowledgements

This work was funded by the US National Science Foundation under grant no. CHE-1566538 and CHE-1954808. The UC Berkeley Molecular Graphics and Computation Facility is supported by the National Institutes of Health under grant no. S10-OD023532. We thank Boulder Scientific Co. for a generous donation of chemicals.

Notes and references

1 B. Marciniec, Catalysis of Hydrosilylation of Carbon-Carbon Multiple Bonds: Recent Progress, *Silicon Chem.*, 2003, **1**, 155–175.
2 M. A. Brook, *Silicon in Organic, Organometallic, and Polymer Chemistry*, A Wiley-Interscience Publication, Wiley, 2000.
3 L. N. Lewis, J. Stein, Y. Gao, R. E. Colborn and G. Hutchins, Platinum Catalysts Used in the Silicone Industry, *Platinum Met. Rev.*, 1997, **41**, 66–75.
4 A. J. Holwell, Global Release Liner Industry Conference 2008, *Platinum Met. Rev.*, 2008, **52**, 243–246.
5 X. Du and Z. Huang, Advances in Base-Metal-Catalyzed Alkene Hydrosilylation, *ACS Catal.*, 2017, **7**, 1227–1243.
6 M. D. Greenhalgh, A. S. Jones and S. P. Thomas, Iron-Catalysed Hydrofunctionalisation of Alkenes and Alkynes, *ChemCatChem*, 2015, **7**, 190–222.
7 J. Y. Wu, B. N. Stanzl and T. A. Ritter, Strategy for the Synthesis of Well-Defined Iron Catalysts and Application to Regioselective Diene Hydrosilylation, *J. Am. Chem. Soc.*, 2010, **132**, 13214–13216.
8 A. M. Tondreau, C. C. H. Atienza, K. J. Weller, S. A. Nye, K. M. Lewis, J. G. P. Delis and P. J. Chirik, Iron Catalysts for Selective Anti-Markovnikov Alkene Hydrosilylation Using Tertiary Silanes, *Science*, 2012, **335**, 567–571.
9 K. Kamata, A. Suzuki, Y. Nakai and H. Nakazawa, Catalytic Hydrosilylation of Alkenes by Iron Complexes Containing Terpyridine Derivatives as Ancillary Ligands, *Organometallics*, 2012, **31**, 3825–3828.
10 A. M. Tondreau, C. C. H. Atienza, J. M. Darmon, C. Milsmann, H. M. Hoyt, K. J. Weller, S. A. Nye, K. M. Lewis, J. Boyer, J. G. P. Delis, E. Lobkovsky and P. J. Chirik, Synthesis, Electronic Structure, and Alkene Hydrosilylation Activity of Terpyridine and Bis(Imino) Pyridine Iron Dialkyl Complexes, *Organometallics*, 2012, **31**, 4886–4893.
11 M. D. Greenhalgh, D. J. Frank and S. P. Thomas, Iron-Catalysed Chemo-, Regio-, and Stereoselective Hydrosilylation of Alkenes and Alkynes Using a Bench-Stable Iron(II) Pre-Catalyst, *Adv. Synth. Catal.*, 2014, **356**, 584–590.
12 M.-Y. Hu, Q. He, S.-J. Fan, Z.-C. Wang, L.-Y. Liu, Y.-J. Mu, Q. Peng and S.-F. Zhu, Ligands with 1,10-Phenanthroline Scaffold for Highly Regioselective Iron-Catalyzed Alkene Hydrosilylation, *Nat. Commun.*, 2018, **9**, 221.
13 J. Sun and L. Deng, Cobalt Complex-Catalyzed Hydrosilylation of Alkenes and Alkynes, *ACS Catal.*, 2016, **6**, 290–300.
14 B. Cheng, P. Lu, H. Zhang, X. Cheng and Z. Lu, Highly Enantioselective Cobalt-Catalyzed Hydrosilylation of Alkenes, *J. Am. Chem. Soc.*, 2017, **139**, 9439–9442.
15 C. Wang, W. J. Teo and S. Ge, Cobalt-Catalyzed Regiodivergent Hydrosilylation of Vinylarenes and Aliphatic Alkenes: Ligand- and Silane-Dependent Regioselectivities, *ACS Catal.*, 2017, **7**, 855–863.
16 X. Du, W. Hou, Y. Zhang and Z. Huang, Pincer Cobalt Complex-Catalyzed Z-Selective Hydrosilylation of Terminal Alkynes, *Org. Chem. Front.*, 2017, **4**, 1517–1521.
17 I. Buslov, J. Becouse, S. Mazza, M. Montandon-Clerc and X. Hu, Chemoselective Alkene Hydrosilylation Catalyzed by Nickel Pincer Complexes, *Angew. Chem., Int. Ed.*, 2015, **54**, 14523–14526.
18 M. I. Lipschutz and T. D. Tilley, Synthesis and Reactivity of a Conveniently Prepared Two-Coordinate Bis(Amido) Nickel(II) Complex, *Chem. Commun.*, 2012, **48**, 7146–7148.
19 I. Buslov, F. Song and X. Hu, An Easily Accessed Nickel Nanoparticle Catalyst for Alkene Hydrosilylation with Tertiary Silanes, *Angew. Chem., Int. Ed.*, 2016, **55**, 12295–12299.
20 Y. Nakajima, K. Sato and S. Shimada, Development of Nickel Hydrosilylation Catalysts, *Chem. Rec.*, 2016, **16**, 2379–2387.

21 I. Pappas, S. Treacy and P. J. Chirik, Alkene Hydrosilylation Using Tertiary Silanes with α-Diimine Nickel Catalysts. Redox-Active Ligands Promote a Distinct Mechanistic Pathway from Platinum Catalysts, *ACS Catal.*, 2016, **6**, 4105–4109.

22 Chirik's (^{iPr}PDI)Fe(N_2)$_2$ catalyst shows slightly higher activities (TOF for 1-hexene: 364 mol h^{-1}), but lower selectivity for terminal olefins. See: S. C. Bart, E. Lobkovsky and P. J. Chirik, Preparation and Molecular and Electronic Structures of Iron(0) Dinitrogen and Silane Complexes and Their Application to Catalytic Hydrogenation and Hydrosilation, *J. Am. Chem. Soc.*, 2004, **126**, 13794–13807.

23 H. A. Brunner, New Hydrosilylation Mechanism - New Preparative Opportunities, *Angew. Chem., Int. Ed.*, 2004, **43**, 2749–2750.

24 P. B. Glaser and T. D. Tilley, Catalytic Hydrosilylation of Alkenes by a Ruthenium Silylene Complex. Evidence for a New Hydrosilylation Mechanism, *J. Am. Chem. Soc.*, 2003, **125**, 13640–13641.

25 R. Waterman, P. G. Hayes and T. D. Tilley, Synthetic Development and Chemical Reactivity of Transition-Metal Silylene Complexes, *Acc. Chem. Res.*, 2007, **40**, 712–719.

26 M. E. Fasulo, M. C. Lipke and T. D. Tilley, Structural and Mechanistic Investigation of a Cationic Hydrogen-Substituted Ruthenium Silylene Catalyst for Alkene Hydrosilation, *Chem. Sci.*, 2013, **4**, 3882–3887.

27 E. Calimano and T. D. Tilley, Synthesis and Structure of PNP-Supported Iridium Silyl and Silylene Complexes: Catalytic Hydrosilation of Alkenes, *J. Am. Chem. Soc.*, 2009, **131**, 11161–11173.

28 C. Beddie and M. B. Hall, A Theoretical Investigation of Ruthenium-Catalyzed Alkene Hydrosilation: Evidence to Support an Exciting New Mechanistic Proposal, *J. Am. Chem. Soc.*, 2004, **126**, 13564–13565.

29 C. Beddie, M. B. Hall and M. B. Do, B3LYP and CCSD(T) Predict Different Hydrosilylation Mechanisms? Influences of Theoretical Methods and Basis Sets on Relative Energies in Ruthenium-Silylene-Catalyzed Ethylene Hydrosilylation, *J. Phys. Chem. A*, 2006, **110**, 1416–1425.

30 M. C. Lipke, A. L. Liberman-Martin and T. D. Tilley, Electrophilic Activation of Silicon-Hydrogen Bonds in Catalytic Hydrosilations, *Angew. Chem., Int. Ed.*, 2017, **56**, 2260–2294.

31 M. C. Lipke and T. D. Tilley, Hypercoordinate Ketone Adducts of Electrophilic η^3-H_2SiRR' Ligands on Ruthenium as Key Intermediates for Efficient and Robust Catalytic Hydrosilation, *J. Am. Chem. Soc.*, 2014, **136**, 16387–16398.

32 M. C. Lipke and T. D. Tilley, High Electrophilicity at Silicon in η^3-Silane σ-Complexes: Lewis Base Adducts of a Silane Ligand, Featuring Octahedral Silicon and Three Ru-H-Si Interactions, *J. Am. Chem. Soc.*, 2011, **133**, 16374–16377.

33 B. V. Mork and T. D. Tilley, Synthons for Coordinatively Unsaturated Complexes of Tungsten, and Their Use for the Synthesis of High Oxidation-State Silylene Complexes, *J. Am. Chem. Soc.*, 2004, **126**, 4375–4385.

34 P. B. Glaser and T. D. Tilley, Synthesis and Reactivity of Silyl and Silylene Ligands in the Coordination Sphere of the 14-Electron Fragment Cp*(^{i}Pr$_3$P)Os$^+$, *Organometallics*, 2004, **23**, 5799–5812.

35 M. E. Fasulo, P. B. Glaser and T. D. Tilley, Cp*(P^{i}Pr$_3$)RuOTf: A Reagent for Access to Ruthenium Silylene Complexes, *Organometallics*, 2011, **30**, 5524–5531.

36 P. W. Smith and T. D. Tilley, Silane-Allyl Coupling Reactions of Cp*(^{i}Pr$_2$MeP)Fe(η^3-allyl)} and Synthetic Access to the Hydrido-Dinitrogen Complex Cp*(^{i}Pr$_2$MeP)FeH(N_2), *Organometallics*, 2015, **34**, 2134–2138.

37 P. W. Smith and T. D. Tilley, Base-Free Iron Hydrosilylene Complexes *via* an α-Hydride Migration That Induces Spin Pairing, *J. Am. Chem. Soc.*, 2018, **140**, 3880–3883.

38 T. Hatanaka, Y. Ohki and K. Tatsumi, Synthesis of Coordinatively Unsaturated Half-Sandwich Iron-Silyl Complexes with an N-Heterocyclic Carbene Ligand and Their Reactions with H_2, *Eur. J. Inorg. Chem.*, 2013, 3966–3971.

39 D. V. Gutsulyak, L. G. Kuzmina, J. A. K. Howard, S. F. Vyboishchikov and G. I. Nikonov, Cp(Pri$_2$MeP)FeH_2SiR_3: Nonclassical Iron Silyl Dihydride, *J. Am. Chem. Soc.*, 2008, **130**, 3732–3733.

40 X. Du, Y. Zhang, D. Peng and Z. Huang, Base-Metal-Catalyzed Regiodivergent Alkene Hydrosilylations, *Angew. Chem., Int. Ed.*, 2016, **55**, 6671–6675.

41 B. Cheng, W. Liu and Z. Lu, Iron-Catalyzed Highly Enantioselective Hydrosilylation of Unactivated Terminal Alkenes, *J. Am. Chem. Soc.*, 2018, **140**, 5014–5017.

42 A. J. Challinor, M. Calin, G. S. Nichol, N. B. Carter and S. P. Thomas, Amine-Activated Iron Catalysis: Air- and Moisture-Stable Alkene and Alkyne Hydrofunctionalization, *Adv. Synth. Catal.*, 2016, **358**, 2404–2409.

43 D. Peng, Y. Zhang, X. Du, L. Zhang, X. Leng, M. D. Walter and Z. Huang, Phosphinite-Iminopyridine Iron Catalysts for Chemoselective Alkene Hydrosilylation, *J. Am. Chem. Soc.*, 2013, **135**, 19154–19166.

44 P. G. Hayes, C. Beddie, M. B. Hall, R. Waterman and T. D. Tilley, Hydrogen-Substituted Osmium Silylene Complexes: Effect of Charge Localization on Catalytic Hydrosilation, *J. Am. Chem. Soc.*, 2006, **128**, 428–429.

45 M. A. Rankin, D. F. MacLean, G. Schatte, R. McDonald and M. Stradiotto, Silylene Extrusion from Organosilanes *via* Double Geminal Si–H Bond Activation by a Cp*Ru(κ^2-P,N)$^+$ Complex: Observation of a Key Stoichiometric Step in the Glaser-Tilley Alkene Hydrosilylation Mechanism, *J. Am. Chem. Soc.*, 2007, **129**, 15855–15864.